PCCP

PAPER

Ab initio study of TaON, an active photocatalyst under visible light irradiation

Cite this: *Phys. Chem. Chem. Phys.*, 2014, **16**, 10558

A. H. Reshak[ab]

Tantalum oxynitride has been studied as an active photocatalyst under visible light, using a full potential linearized augmented plane wave method within the framework of density functional theory. The electronic and optical properties of TaON are calculated using local density approximation (LDA), generalized gradient approximation (GGA), Engel–Vosko generalized gradient approximation (EVGGA) and the modified Becke–Johnson (mBJ) potential approximation to describe the exchange–correlation potential. The calculated band gap value obtained by the mBJ approximation approach (2.5 eV) is very close to the experimental result (2.5 eV). We found that hybridization among the Ta-d, O-p and N-p states results in the formation of a covalent bond between Ta–N and Ta–O. The calculated optical properties confirm that the TaON is an active photocatalyst under visible light irradiation. TaON has a high dielectric constant and the components show anisotropy in the energy range between 3.0 eV and 10.0 eV. A high refractive index of 2.47 at 632.8 nm is obtained which shows better agreement with the experimental value (2.5 at 632.8 nm) than previous results.

Received 19th January 2014,
Accepted 1st March 2014

DOI: 10.1039/c4cp00285g

www.rsc.org/pccp

1. Introduction

Materials science has influenced several industrial fields, enabling the design of multifunctional materials. These materials have many applications in different industrial branches. A single material with many desirable properties would be suitable to meet the challenges presented. Promising multifunctional materials include transitional metal oxynitrides (TM-O-N), which are technologically important for applications in the field of biocompatible coatings, solar absorbers, electrochromic coatings, nanocrystalline solar cells and catalysts.[1–4] Compared to pure oxides, it has been found that TM-O-N (TM = Ta, Hf, Zr, or Ti) have improved optical properties.[5] One of the TM-O-N is tantalum oxynitride (TaON), which covers a wide range of technological applications including decorative coatings,[6] gate oxide microelectronic devices,[7,8] charge capacitors in dynamic random access memory devices[9] and visible light photocatalysts.[10–13] Tantalum oxynitride has been discussed by Brauer and Weidlein.[14] The monoclinic baddeleyite structure, β-TaON, is the only confirmed and stable polymorph of TaON. Ordered arrangement of O and N in β-TaON was observed using a powder neutron diffraction technique.[15] β-TaON was synthesized from the material β-Ta_2O_5 by treating with ammonia gas at 800 °C. The existing α-TaON hexagonal polymorph, proposed by Buslaev *et al.*,[16] was rejected on the basis of quantum chemical calculations.[17] A metastable polymorph, γ-TaON, is a new phase suggested by Schilling *et al.*[18] The outshining property of TaON is its high dielectric constant, which enables gate oxides to increase their capacitance despite a decrease in their thickness.[19] A lot of work has been done to calculate the structure, stability of its polymorphs, electronic structure and high pressure phases.[17,18,20–24] Clean and recyclable hydrogen energy can be obtained by splitting water into its components using photocatalysts. Photocatalysts are not only important due to the production of hydrogen by dissociating water, but they also have the ability to degrade waste products to keep the environment clean.[25] Most materials have wide band gaps which are excited under ultraviolet light irradiation. To absorb visible light, the band gap should be small. Metal (cations)[26–31] doping has been used to reduce the band gap. However, the trend of doping nonmetals (anions)[32–36] into these wide band gap semiconductors has now increased. A large band gap is one of the reasons that disqualifies metal oxides from showing photocatalytic activity in the visible region of the electromagnetic spectrum (*e.g.* TiO_2[37]). Visible light photocatalytic activity is mostly observed for metal oxynitrides such as N-doped TiO_2[34] and $(Ga_{1-x}Zn_x)(N_{1-x}O_x)$.[38–40] TaON can be excited for photocatalysis at wavelengths up to 530 nm and the calculated band gap is 2.3 eV.[10–13] Chun *et al.* used X-ray, ultraviolet photoelectron spectroscopy and electrochemical analysis to find the band position of TaON.[13] The crystal structure of TaON has been studied by neutron powder diffraction using the Rietveld method at 4 K, confirming anion ordering.[41]

[a] *New Technologies - Research Center, University of West Bohemia, Univerzitni 8, 306 14 Pilsen, Czech Republic. E-mail: maalidph@yahoo.co.uk; Tel: +420 777 729 583*

[b] *Center of Excellence Geopolymer and Green Technology, School of Material Engineering, University Malaysia Perlis, 01007 Kangar, Perlis, Malaysia*

Fang *et al.*[20] have calculated the band structure of TaON and shown that there is hybridization between the anion 2-p state and Ta-5d states. Neutron diffraction has been used to investigate the crystal structure of TaON in order to confirm the anion ordering.[42] Synchrotron powder diffraction has been applied to accurately measure the crystal structure and electron density.[42] Orhan *et al.*[43] studied the synthesis and energetics of the yellow TaON; the diffuse reflectance spectra show that the measured band gap is 2.4 eV. Al-Aqtash *et al.*[44] reported the results of *ab initio* studies of the electronic structure of TaON-based alloys. They show that the position of the conduction and the valence bands can be modified by varying the oxygen and nitrogen concentrations in $TaO_{1-x}N_{1+x}$. They found that the static refractive index of TaON has a value of 2.47, which is similar to the experimental results (over 2.5 at a wavelength of 632.8 nm) for TaON films.

From the above, we notice that there is a dearth of information about the electronic structure and optical properties of tantalum oxynitride as a visible light photocatalyst. Therefore we thought it would be worthwhile to perform comprehensive theoretical calculations based on the self-consistent first principle full potential calculations to obtain comprehensive information about the crystal structure, electronic band structure, chemical bonding, electronic charge density and optical properties such as the absorption coefficient, reflectivity, and dielectric function of tantalum oxynitride.

2. Theoretical calculations

In this work we discuss the crystal structure, electronic band structure, electronic charge density distribution and optical properties of tantalum oxynitride in detail. The ground state properties of TaON are calculated using a full potential linearized augmented plane wave (FP-LAPW) method as implemented in a WIEN2K package.[45] In the FP-LAPW method, the unit cell is split into an atomic sphere (MT) and an interstitial region (IR). The cutoff parameter, $R_{MT}K_{max}$, is set to 7.0 for the convergence of the basis set, where R_{MT} is the smallest muffin-tin radii and K_{max} represents the largest value of the vector K. The calculations were performed using 1377 **K** points in the irreducible Brillouin zone (BZ). We have used four forms of approximation, namely, local density approximation (LDA), generalized gradient approximation (GGA), Engel–Vosko generalized gradient approximation (EVGGA) and the modified Becke–Johnson (mBJ) potential approximation to describe the exchange–correlation potential. The self-consistent convergence accuracy was set at 10^{-4} Ry. The criterion for convergence of the maximum force among atoms is 1 mRy per a.u. at which the structural geometry is relaxed. The modified Becke–Johnson potential approximation approach is considered to be better than LDA, GGA and EVGGA in obtaining a better band gap value that is mostly underestimated by LDA, GGA and EVGGA.[46,47] We would like to mention here that in our previous studies,[48–53] we have calculated the energy band gap using the FPLAPW method with the mBJ potential approximation approach for several systems whose energy band gaps are known experimentally. We found very good agreement with the experimental data.

Table 1 Calculated band gap of TaON at different values of mixing factor for mBJ calculations

	Mixing factor	Band gap value (E_g)	Exp. E_g
mBJ	0.60	3.14	**2.50**[a]
	0.50	3.15	
	0.40	3.19	
	0.30	3.00	
	0.20	3.18	
	0.10	3.10	
	0.05	2.80	
	0.01	2.70	
	0.001	**2.50**	
	0.005	2.20	

[a] Ref. 54.

Thus we believe that the calculations reported in this paper would produce very accurate and reliable results. Good photocatalytic materials should possess an energy gap less than 3.0 eV to efficiently utilize solar energy, which is very crucial and promising for clean and sustainable energy. Thus, a large band gap is one of the reasons that disqualifies metal oxides from showing photocatalytic activity in the visible region. The investigated compound, TaON, can be excited for photocatalysis at wavelengths up to *ca.* 530 nm and the calculated band gap is 2.3 eV,[10–13] while the measured band gap is 2.5 eV.[54] Therefore it is very important to obtain an energy gap closer to the measured one. Hence, the mBJ potential approximation approach is proposed. It is well-known the mBJ calculation is very sensitive to values of the mixing factor (mixing FACTOR for BROYD/PRATT scheme). Thus one has to be careful when selecting the mixing factor value which can bring the calculated value of the energy gap closer to the experimental ones. Therefore, in this work we have investigated the effect of changing the mixing factor on the value of the energy gap and hence on the electronic structure. We should emphasize that in general, when reducing the value of the mixing factor, there is a clear reduction in the energy gap's value. Trying different mixing factor values helped us to tailor the calculated energy gap closer to the experimental ones (see Table 1). Therefore, selecting the correct mixing factor for the mBJ potential approximation makes the DFT calculation more reliable and allows the calculation of band gaps with accuracy similar to the very expensive GW calculations. This is a local approximation to an atomic "exact-exchange" potential and a screening term. In particular, the density of states (DOS) and optical properties are calculated using the mBJ potential approximation approach. The only stable crystal of TaON is a monoclinic baddeleyite structure with space group $P2_1/c$[42] (see Fig. 1). Lattice parameters and atomic positions are listed in Table 2.[52] Ordered arrangement of anions occurs in alternate layers of OTa_3 (triangles) and NTa_4 (tetrahedra).[42]

3. Result and discussions

3.1 Band structure and density of states

The calculated electronic energy band structure, using different schemes, is displayed in Fig. 2(a–d). From Fig. 2, one can see that the conduction band minimum (CBM) is located at point *Y*

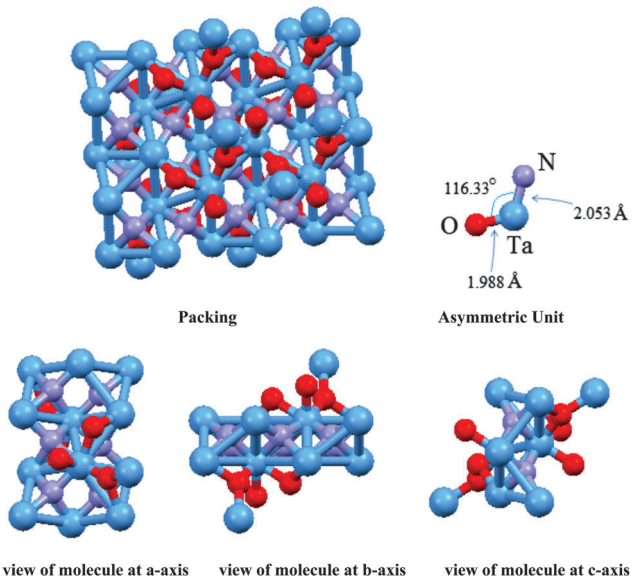

Fig. 1 Unit cell structure of TaON.

Table 2 Lattice constants and atomic coordinates of TaON[42]

		a	*b*	*c*
Lattice parameters (Å)		4.94941	5.01662	5.16430
		Atomic positions		
Atom	Wyckoff site	*x*	*y*	*z*
Ta	4e	0.29197	0.04477	0.21486
O	4e	0.0662	0.3273	0.3443
N	4e	0.4447	0.7557	0.4808

of the BZ, while the valence band maximum (VBM) is located at the center of the BZ, resulting in an indirect band gap. The implication of using LDA, GGA, EVGGA and the mBJ potential approximation is that we get a better value of energy band gap every time. The energy band gap values are 1.93 eV (LDA), 2.05 eV (GGA), 2.42 eV (EVGGA) and 2.50 eV (mBJ). The underestimation of band gaps by DFT is common, which exists due to the limitation of predicting conduction band properties.[55] As the value of the energy gap is an important issue for photocatalysis, we therefore paid more attention to getting the energy gap closer to the experimental values. For this reason, different mixing factors were chosen for calculating the energy gap using the mBJ scheme, as shown in Table 1. Looking at Table 1, one can see that the mixing factor 0.001 brings the calculated band gap (2.5 eV) close to the experimental value, 2.5 eV,[54] and is better than previous theoretical values of 1.8 eV[17–19,56,57] and 1.92 eV.[19]

Useful information can be gained from partial density of states (PDOS), such as hybridization of states, bonding nature and contribution of orbitals to the electronic band structure. Fig. 3 illustrates the PDOS of Ta, O and N atoms in TaON. The PDOS show that the valence band maximum mostly consists of O-p and N-p states which are strongly hybridized with Ta-d orbitals, while the bottom of the conduction band is composed of a Ta-d state overlap with O-p and N-p. Between −7.0 eV and

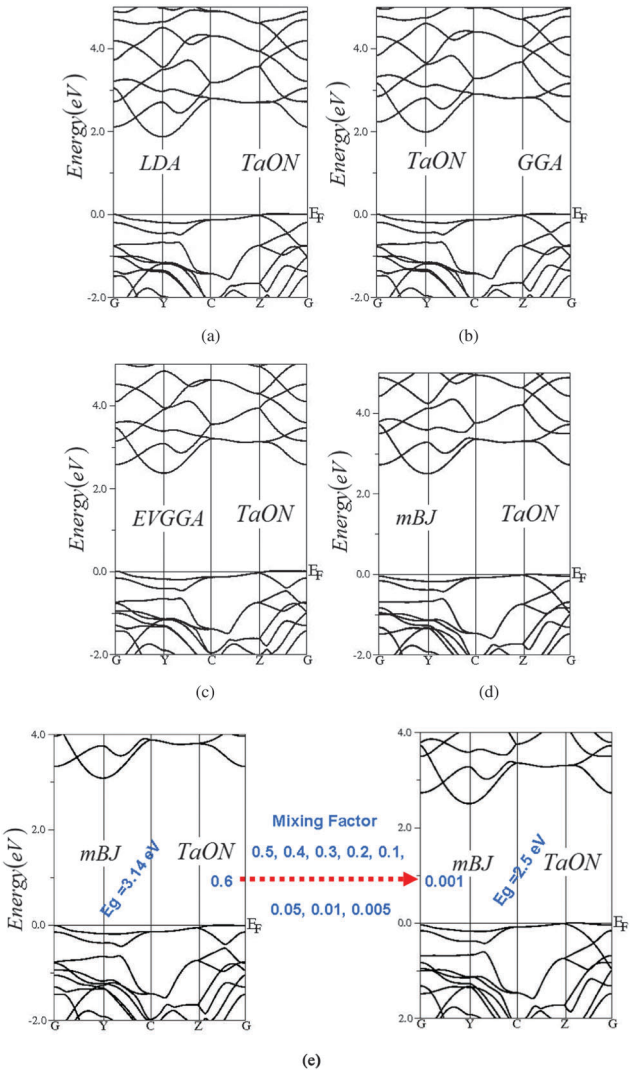

Fig. 2 Calculated band structure of TaON.

−1.0 eV, the O-p state plays a dominant role and some contribution from O-p and Ta-d is also involved. The N-s orbital mainly contributes between −13.0 eV and −15.0 eV and a small participation from the Ta-d state can also be observed. The Ta-f state appears at a much lower energy range around −19.0 eV. At a higher energy range, between 2.5 eV and 11.0 eV, the dominant occupied state is Ta-d with a small contribution from O-p and N-p. Strong hybridization means potential covalent bonding and a less ionic character. A covalent bond between O or N and the Ta atom can be seen when the O-p and N-p states hybridized with Ta-d between −7.0 eV and 0.0 eV. Dispersion of the valence band increased up to −7.0 eV due to the strong hybridization between the O, N and Ta orbitals. As a result, the VBM is raised, which makes TaON active under visible light irradiation.

3.2 Electronic charge density

The electronic charge density was calculated in the (101) and (−101) crystallographic planes by using the mBJ potential appromixation approach. One can easily predict the bonding

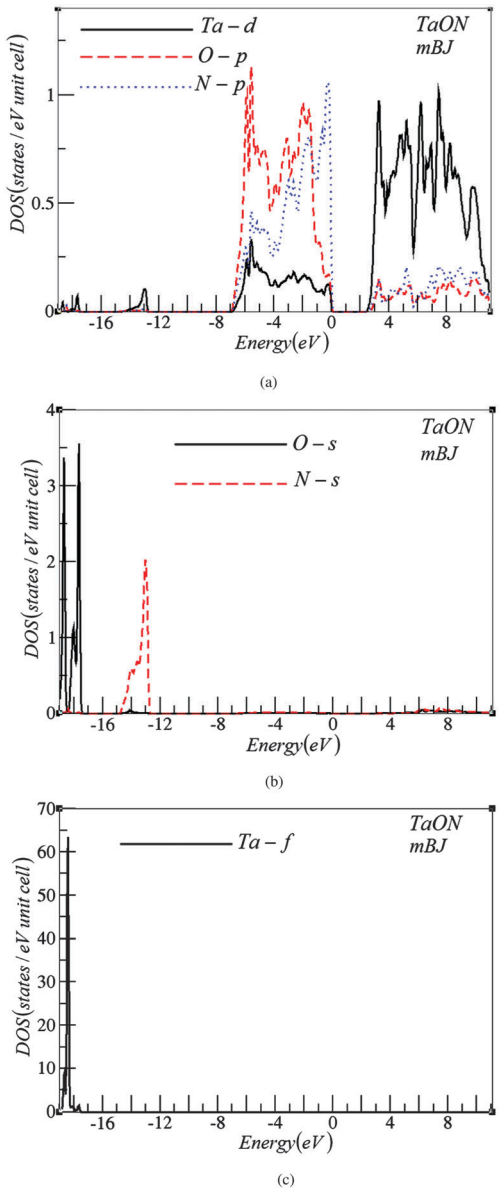

Fig. 3 Calculated total density of states (states/eV unit cell) and PDOS of TaON.

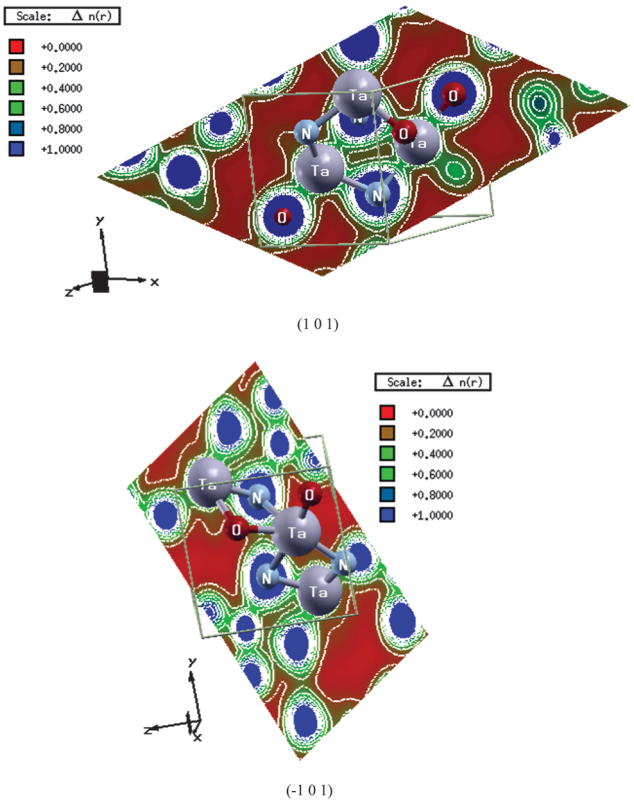

Fig. 4 Electronic charge density of TaON.

Table 3 Calculated bond lengths of TaON using the mBJ potential

	Bond length (Å)	
Bond	This work	Other[19]
O–Ta	2.060, 2.147, 1.988	2.147, 1.988, 2.060
N–Ta	2.053, 2.147, 2.069, 2.118	2.147, 2.188, 2.069, 2.053

nature and charge transfer between atoms from the electronic charge density; a greater electronegativity difference (ΔEN) assures ionic bonding and smaller ΔEN demonstrates the presence of a covalent bond between atoms. The electronegativity values of Ta, O and N are 1.5, 3.44 and 3.04 respectively. The ΔEN between O and Ta is 1.94 and 0.4 between O and N, which indicates the covalent nature of the bonds between these atoms. From the electronegativity difference we can find out the percentage ionic character. The percent ionicity from the ΔEN between O and Ta is 44.21%, resulting in a greater percentage of covalency, 55.79%. Also, the percentage ionic character (6.96%) between O and N is less than the covalency (93.04%). The covalent bond is attributed to the existence of strong hybridization between the O-p, N-p and Ta-d states. The effect of most electronegative elements to attract electrons towards itself can easily be seen from the charge density plot in the (101) and (−101) crystallographic planes. From the thermoscale, colors represent different charge concentration areas. A blue color represents the maximum charge, which means that the maximum charge gathered around oxygen and nitrogen is highly electronegative. Electron charge density also helps to sort out the anisotropy between planes (Fig. 4). We find considerable anisotropy between the (101) and (−101) crystallographic plane as both the planes show a contribution of different numbers of atoms to the electron charge density. In the (101) plane, Ta, O and N contribute to the electron charge density, while in the (−101) plane, only Ta and N are shown. The bond length values are calculated and listed in Table 3.

3.3 Optical properties

The optical properties of TaON are calculated by the dielectric function $\varepsilon(\omega) = \varepsilon_1(\omega) + I\varepsilon_2(\omega)$. The Kramer–Kronig relation is used to obtain the real parts of the dielectric function from imaginary ones. Optical properties such as reflectivity $R(\omega)$, absorption coefficient $I(\omega)$, energy loss function $L(\omega)$, refractive index $n(\omega)$ and extinction coefficient $k(\omega)$ are calculated from the dielectric constant. In order to show the influence of using

different exchange–correlations on the optical properties of TaON, we have calculated the average dielectric constant $\varepsilon_2^{average}(\omega)$ and $\varepsilon_1^{average}(\omega)$ using LDA, GGA, EVGGA and the mBJ potential (see Fig. 5a and b). It is clear that the mBJ potential approximation approach shows the correct optical gap. The values of $\varepsilon_1^{average}(0)$ are listed in Table 3, which show that a smaller energy gap yields a larger $\varepsilon_1(0)$ value. This could be explained on the basis of the Penn model.[58] Penn proposed a relationship between $\varepsilon(0)$ and E_g, $\varepsilon(0) \approx 1 + (\hbar\omega_P/E_g)^2$. E_g is an averaged energy gap which could be related to the real energy gap. It is clear that $\varepsilon(0)$ is inversely proportional to E_g. Hence, a smaller E_g yields a larger $\varepsilon(0)$. Looking at Fig. 5a and b, one can conclude that the mBJ potential approximation approach produces a better band gap in comparison to LDA, GGA and EVGGA. Therefore, we decided to show only the results obtained by the mBJ approach.

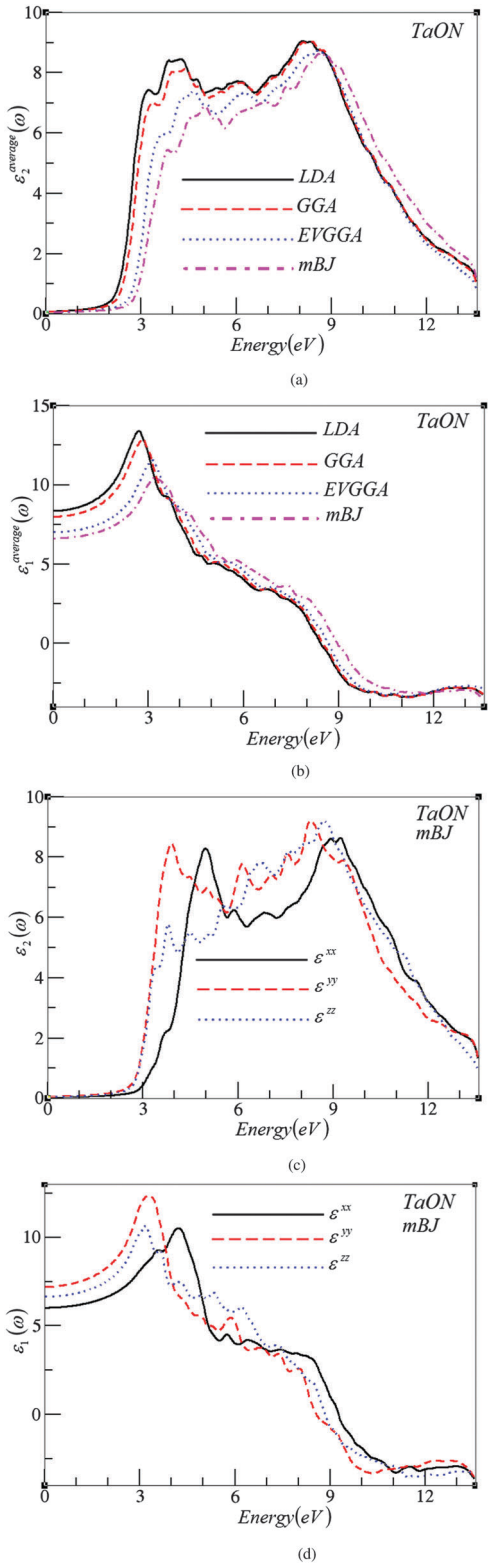

Fig. 5 Calculated $\varepsilon_2^{average}(\omega)$, $\varepsilon_2(\omega)$, $\varepsilon_1^{average}(\omega)$ and $\varepsilon_1(\omega)$ for TaON.

Fig. 5c shows $\varepsilon_2(\omega)$ using the mBJ approach, the critical points (threshold points) of $\varepsilon_2^{xx}(\omega)$ and $\varepsilon_2^{yy}(\omega)$ are 2.4 and 2.5 for $\varepsilon_2^{zz}(\omega)$. The spectral structures of the three components show two main peaks, one located at lower energies around 4.0 eV for $\varepsilon_2^{xx}(\omega)$ and $\varepsilon_2^{yy}(\omega)$ and around 5.0 eV for $\varepsilon_2^{zz}(\omega)$. The second peak is located at higher energies around 9.0 eV for both $\varepsilon_2^{xx}(\omega)$ and $\varepsilon_2^{yy}(\omega)$ and at 9.5 eV for $\varepsilon_2^{zz}(\omega)$. There is a considerable anisotropy between the three compounds. The real part, $\varepsilon_1(\omega)$, calculated using the mBJ potential, which also confirms the considerable anisotropy between $\varepsilon_1^{xx}(\omega)$, $\varepsilon_1^{yy}(\omega)$ and $\varepsilon_1^{zz}(\omega)$. The calculated values of $\varepsilon_1^{xx}(0)$, $\varepsilon_1^{yy}(0)$ and $\varepsilon_1^{zz}(0)$ using LDA, GGA, EVGGA and mBJ are listed in Table 4 along with the previous theoretical CASTEP-LDA calculations.[19] The uniaxial anisotropy $\delta\varepsilon = (\varepsilon_0^{\parallel} - \varepsilon_0^{\perp})/\varepsilon_0^{tot}$ which indicates the strong anisotropy of the dielectric function, is calculated and listed in Table 4. The transition between the Ta-d and p states of the anions mainly contributes to the peaks which occur in the imaginary part, $\varepsilon_2(\omega)$, at around 3.0 eV and 9.0 eV.

The reflectivity spectrum, $R(\omega)$, is plotted as a function of wavelength (see Fig. 6a) in which $R^{yy}(\omega)$ remains dominant throughout the spectrum. The maximum reflectivity value for all components occurs at about 90.0 nm. Two minor peaks at around 250 nm for $R^{xx}(\omega)$ and 350 nm for $R^{yy}(\omega)$ were also observed. Above 450 nm, the spectra of all the components remain constant. The absorption coefficient, $I(\omega)$, measures the penetration of light through materials before it gets absorbed. We have calculated the absorption coefficient in terms of wavelength (nm) (see Fig. 6b). The $I(\omega)$ rapidly increases above 90 nm and reaches its maximum value at around 140 nm.

Table 4 Calculated $\varepsilon_1^{average}(0)$, $\varepsilon_1^{xx}(0)$, $\varepsilon_1^{yy}(0)$, $\varepsilon_1^{zz}(0)$, $n^{xx}(0)$, $n^{yy}(0)$, and $n^{zz}(0)$

	LDA	GGA	EVGGA	mBJ
$\varepsilon_1^{average}(0)$	8.38, 9.0[a]	8.00	7.01	6.61
$\varepsilon_1^{xx}(0)$	7.56	7.30	6.40	6.02
$\varepsilon_1^{yy}(0)$	9.30	8.80	7.70	7.22
$\varepsilon_1^{zz}(0)$	8.30	7.90	6.90	6.65
$\delta\varepsilon = (\varepsilon_0^{\parallel} - \varepsilon_0^{\perp})/\varepsilon_0^{tot}$	−0.015	−0.018	−0.021	0.004
$n^{xx}(0)$	2.75	2.69	2.53	2.45
$n^{yy}(0)$	3.04	2.97	2.77	2.68
$n^{zz}(0)$	2.87	2.81	2.64	2.58
$n^{average}(0)$	2.88, 3.0[a]	2.82	2.64	2.57
$n^{average}(\omega)$				2.47 at 632.8 nm
$n^{average}(\omega)$exp.	2.5[b] at 632.8 nm			

[a] Ref. 19. [b] Ref. 8.

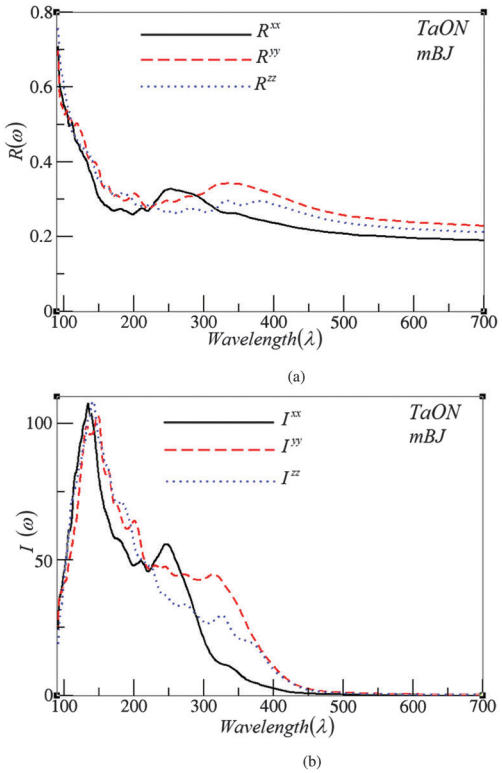

Fig. 6 Reflectivity and absorption coefficient. (a) $R(\omega)$, (b) $I(\omega)$.

Absorption also occurs in the visible region, which indicates that TaON is an active photocatalyst under visible light irradiation. The TaON crystal almost behaves as a transparent crystal in the higher wavelength light. The absorption band extends from 90 nm to 450 nm.

The refractive index $n(\omega)$, extinction coefficient $k(\omega)$ and energy loss function $L(\omega)$ are calculated and shown in Fig. 7(a–c). The complex refractive index ($\tilde{n}(\omega) = n(\omega) + ik(\omega)$) describes the refraction, as well as the absorption, of the compounds. It consists of two parts; the real part, $n(\omega)$, is just the ordinary refractive index, while the other part, $k(\omega)$, is the extinction which describes the loss of photon energy as it propagates through the optical medium. As these compounds have monoclinic symmetry, five tenser components are required to completely describe the optical properties. We will concentrate only on the major components which are parallel to the x, y and z axes.

The x, y, and z components of the refractive index and extinction coefficient as a function of energy are plotted in Fig. 7(a) and (b). The refractive indices at the static limits, $n^{xx}(0)$, $n^{yy}(0)$ and $n^{zz}(0)$, are calculated and listed in Table 4. The average value of the refractive index of TaON is 2.57 at the static limit, $n^{\text{average}}(0)$, and 2.47 at 632.8 nm. Our calculations show better agreement with the experimental value, 2.5 at 632.8 nm,[8] than another theoretical value, 3.0.[19] The refractive indices increased beyond the zero frequency limits and reached their maximum values. Beyond the maximum value they start to decrease and with a few oscillations they go beyond unity. In this region ($n < 1$), the phase velocity of the photons increases

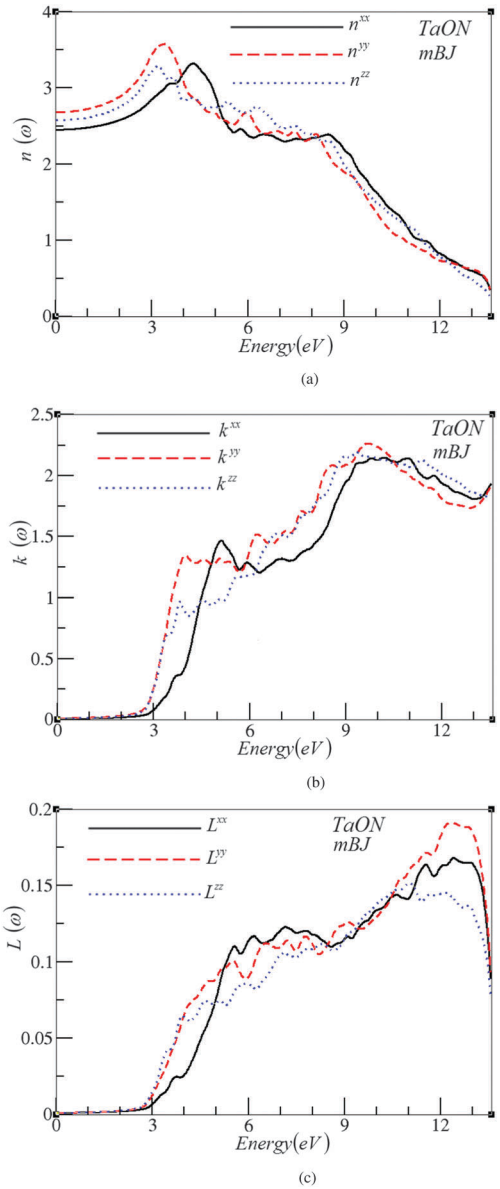

Fig. 7 Refractive index $n(\omega)$, extinction coefficient $k(\omega)$ and energy loss function $L(\omega)$.

to a universal constant (C). However the group velocity is always less than the C, and therefore the relativity relations are not effected.[59] The extinction coefficient, $k(\omega)$, expresses the absorption of compounds. It is seen from Fig. 7b that the absorption edge for $k^{xx}(\omega)$ is 2.7 eV, and 2.5 for $k^{yy}(\omega)$ and $k^{zz}(\omega)$. Beyond the critical points, the absorption increases and reaches the maximum at a particular energy, and then it decreases with small oscillations. The compound shows high absorption in the range between 3.0 and 4.0 eV. The energy loss by the electron as it passes through the crystal is defined by an optical parameter, energy loss function $L(\omega)$. The peaks in the $L(\omega)$ indicate trailing edges in the reflectivity structure, such as the reduction of $R(\omega)$ at a wavelength between 104 nm and 150 nm, which corresponds to the peaks at about 12.5 eV in $L(\omega)$.

4. Conclusions

A full potential linearized augmented plane wave method (FP-LAPW) was used to investigate the structural, electronic and optical properties of TaON. The calculations show that TaON has a band gap value of 2.5 eV obtained using the mBJ potential approximation approach, which matches well with the experimental value. TaON is an indirect band gap semiconductor. In the PDOS, the hybridized anion p and Ta-d orbitals are accountable for the covalent bond between Ta–N and Ta–O. As a consequence of this covalent bond, the valence band dispersion increases and pushes the top of the valence band towards the Fermi level, resulting in a TaON compound that is photocatalytically active under visible light irradiations. TaON bears a high dielectric constant and in the present calculation, the dielectric constant value is presented in Table 4. We found the refractive index to be about 2.47 at 632.8 nm for TaON, which is in good agreement with the experimental value (2.5 at 632.8 nm). The energy loss function and extinction coefficient were also calculated. The peaks in the energy loss function represent a reduction in the trailing edges of the reflectivity spectrum.

Acknowledgements

The results were developed within the CENTEM project, reg. no. CZ.1.05/2.1.00/03.0088, co-funded by the ERDF as part of the Ministry of Education, Youth and Sports OP RDI programme.

References

1 T. I. Tsyganov, M. F. Maitz, E. Wieser, E. Richter and H. Reuther, *Surf. Coat. Technol.*, 2005, **200**, 1041–1044.
2 R. Mientus, R. Grötschel and K. Ellmer, *Surf. Coat. Technol.*, 2005, **200**, 341–345.
3 M. A. Aegerter, *Sol. Energy Mater. Sol. Cells*, 2001, **68**, 401–422.
4 W. Assmann, Th. Reichelt, T. Eisenhammer, H. Huber, A. Mahr, H. Schellinger and R. Wolgemuth, *Nucl. Instrum. Methods Phys. Res., Sect. B*, 1996, **113**, 303–307.
5 S. Venkataraj, D. Severin, S. H. Mohamed, J. Ngaruiya, O. Kappertz and M. Wuttig, *Thin Solid Films*, 2006, **502**, 228–234.
6 F. Vaz, P. Cerqueira, L. Rebouta, S. M. C. Nascimento, E. Alves, P. Goudeau, J. J. P. Riviere, K. Pischow and J. De Rijk, *Thin Solid Films*, 2004, **449**, 447–448.
7 H. Le Dreo, O. Banakh, H. Keppner, P.-A. Steinmann, D. Briand and N. F. de Rooij, *Thin Solid Films*, 2006, **515**, 952–956.
8 K. Kato, H. Toyota, Y. Jin and T. Ono, *Vacuum*, 2009, **83**, 592–595.
9 S. L. Cho, B. S. Kim, H. M. Kim, I. K. Chun and K. B. J. Kim, *J. Electrochem. Soc.*, 2002, **149**, C529.
10 G. Hitoki, T. Takata, J. N. Kondo, M. Hara, H. Kobayashi and K. Domen, *Chem. Commun.*, 2002, 1698–1699.
11 M. Hara, E. Chiba, A. Ishikawa, T. Takata, J. N. Kondo and K. J. Domen, *J. Phys. Chem. B*, 2003, **107**, 13441–13445.
12 M. Hara, G. Hitoki, T. Takata, J. N. Kondo, H. Kobayashi and K. Domen, *Catal. Today*, 2003, **78**, 555–560.
13 W.-J. Chun, A. Ishikawa, H. Fujisawa, T. Takata, J. N. Kondo, M. Hara, M. Kawai, Y. Matsumoto and K. Domen, *J. Phys. Chem. B*, 2003, **107**, 1798–1803.
14 G. Brauer and J. Weidlein, *Angew. Chem.*, 1965, **77**, 913 (*Angew. Chem., Int. Ed. Engl.*, 1965, **4**, 875).
15 D. Armytage and B. E. F. Fender, *Acta Crystallogr., Sect. B: Struct. Crystallogr. Cryst. Chem.*, 1974, **30**, 809–812.
16 Yu. A. Buslaev, G. M. Safronov, V. I. Pachomov, M. A. Glushkova, V. P. Repko, M. M. Ershova, A. N. Zhukov, T. A. Zhdanova, I. Akad and S. S. S. R. Nauk, *Neorg. Mater.*, 1969, **5**, 45–48.
17 M.-W. Lumey and R. Dronskowski, *Z. Anorg. Allg. Chem.*, 2003, **629**, 2173–2179.
18 H. Schilling, A. Stork, E. Irran, H. Wolff, T. Bredow, R. Dronskowski and M. Lerch, *Angew. Chem., Int. Ed.*, 2007, **46**, 2931–2934.
19 P. Li, W. Fan, Y. Li, H. Sun, X. Cheng, X. Zhao and M. Jiang, *Inorg. Chem.*, 2010, **49**, 6917–6924.
20 C. M. Fang, E. Orhan, G. A. de Wijs, H. T. Hintzen, R. A. de Groot, R. Marchand, J.-Y. Saillard and G. J. de With, *J. Mater. Chem.*, 2001, **11**, 1248–1252.
21 M.-W. Lumey and R. Z. Dronskowski, *Z. Anorg. Allg. Chem.*, 2005, **631**, 887–893.
22 H. Wolff, T. Bredow, M. Lerch, H. Schilling, E. Irran, A. Stork and R. Dronskowski, *J. Phys. Chem. A*, 2007, **111**, 2745–2749.
23 T. Bredow, M.-W. Lumey, R. Dronskowski, H. Schilling, J. Pickardt and M. Z. Lerch, *Z. Anorg. Allg. Chem.*, 2006, **632**, 1157–1162.
24 J. E. Lowther, *Phys. Rev. B: Condens. Matter Mater. Phys.*, 2006, **73**, 134110.
25 F. Han, V. S. R. Kambala, M. Srinivasan, D. Rajarathnam and R. Naidu, *Appl. Catal., A*, 2009, **359**, 25.
26 A. P. Singh, S. Kumari, R. Shrivastav, S. Dass and V. R. Satsangi, *Int. J. Hydrogen Energy*, 2008, **33**, 5363.
27 G. J. Shao, *J. Phys. Chem. C*, 2008, **112**, 18677.
28 R. Sasikala, V. Sudarsan, C. Sudakar, R. Naik, T. Sakuntala and S. R. Bharadwaj, *Int. J. Hydrogen Energy*, 2008, **33**, 4966.
29 M. K. Seery, R. George, P. Floris and S. C. J. Phillai, *J. Photochem. Photobiol., A*, 2007, **189**, 258.
30 S. Kim, S.-J. Hwang and W. Choi, *J. Phys. Chem. B*, 2005, **109**, 24260.
31 A. V. Emeline, G. N. Kuzmin and N. Serpone, *Chem. Phys. Lett.*, 2008, **454**, 279.
32 R. Asahi, T. Morikawa, T. Ohwaki, K. Aoki and Y. Taga, *Science*, 2001, **293**, 269.
33 R. Asahi and T. Morikawa, *Chem. Phys.*, 2007, **339**, 57.
34 M. C. Long, W. M. Cai, Z. P. Wang and G. Z. Liu, *Chem. Phys. Lett.*, 2006, **420**, 71.
35 Z. S. Lin, A. Orlov, R. M. Lambert and M. C. Payne, *J. Phys. Chem. B*, 2005, **109**, 20948.
36 K. S. Yang, Y. Dai and B. B. Huang, *J. Phys. Chem. C*, 2007, **111**, 12086.
37 A. Fujishima and K. Honda, *Nature*, 1972, **238**, 37–38.

38 K. Maeda, T. Takata, M. Hara, N. Saito, Y. Inoue, H. Kobayashi and K. J. Domen, *J. Am. Chem. Soc.*, 2005, **127**, 8286–8287.

39 M. Yashima, K. Maeda, K. Teramura, T. Takata and K. Domen, *Chem. Phys. Lett.*, 2005, **416**, 225–228.

40 M. Yashima, K. Maeda, K. Teramura, T. Takata and K. Domen, *Mater. Trans.*, 2006, **47**, 295–297.

41 D. Armytage and B. E. F. Fender, *Acta Crystallogr., Sect. B: Struct. Crystallogr. Cryst. Chem.*, 1974, **30**, 809–812.

42 M. Yashima, Y. Lee and K. Domen, *Chem. Mater.*, 2007, **19**, 588–593.

43 E. Orhan, F. Tessier and R. Marchand, *Solid State Sci.*, 2002, **4**, 1071–1076.

44 N. Al-Aqtash, F. Apostol, W.-N. Mei and R. F. Sabirianov, *J. Solid State Chem.*, 2013, **198**, 337–343.

45 P. Blaha, K. Schwarz, G. K. H. Madsen, D. Kvanicka and J. Luitz, 2001 WIEN2K, An Augmented plane wave + Local Orbital Program for Calculating Crystal Properties Karlheinz Schwarz; Techn. Universitat: Wien, Austria, ISBN: 3-9501031-1-1-2.

46 F. Tran and P. Blaha, Accurate Band Gaps of Semiconductors and Insulators with a Semilocal Exchange-Correlation Potential, *Phys. Rev. Lett.*, 2009, **102**, 226401–226404.

47 S. Guo and B. Liu, *J. Magn. Magn. Mater.*, 2012, **324**, 2410–2415.

48 A. H. Reshak, O. V. Parasyuk, A. O. Fedorchuk, H. Kamarudin, S. Auluck and J. Chysky, *J. Phys. Chem. B*, 2013, **117**, 15220–15231.

49 A. H. Reshak, I. V. Kityk, O. V. Parasyuk, H. Kamarudin and S. Auluck, *J. Phys. Chem. B*, 2013, **117**, 2545–2553.

50 A. H. Reshak, X. Chen, S. Auluck and H. Kamarudin, *Mater. Chem. Phys.*, 2012, **137**, 346–352.

51 A. H. Reshak, X. Chen, S. Auluck and H. Kamarudin, *J. Appl. Phys.*, 2012, **112**, 053526.

52 A. H. Reshak, I. V. Kityk, O. V. Parasyuk, A. O. Fedorchuk, Z. A. Alahmed, N. AlZayed, H. Kamarudin and S. Auluck, *J. Mater. Sci.*, 2013, **48**, 1342–1350.

53 A. H. Reshak and S. A. Khan, *Mater. Res. Bull.*, 2013, **48**, 4555–4564.

54 K. Maeda and K. Domen, *J. Phys. Chem. C*, 2007, **111**, 7851.

55 R. M. Martin, *Electronic Structure: Basic Theory and Practical Methods*, Cambridge University Press, Cambridge, England, 2004.

56 C. Fang, E. Orhan, G. de Wijs, H. Hintzen, R. de Groot, R. Marchand, J. Saillard and G. de With, *J. Mater. Chem.*, 2001, **11**, 1248.

57 M. Yashima, Y. Lee and K. Domen, *Chem. Mater.*, 2007, **19**, 588.

58 D. R. Penn, *Phys. Rev.*, 1962, **128**, 2093.

59 M. Fox, *Optical Properties of Solids*, Oxford University Press, 2001.